

# Ionospheric Propagation Modes Identified using the TIGER HF Radar

Peter L. DYSON, Robert J. NORMAN and Murray L. PARKINSON

**Abstract**—The Tasman International Geospace Environment Radar (TIGER) is a High-Frequency (HF) radar that probes the ionosphere between Tasmania and Antarctica. Its main purpose is to detect direct backscatter from ionospheric irregularities, but it also detects echoes from signals that are reflected from the ionosphere down to the sea, and backscattered so they return to the radar again via the ionosphere. The occurrence characteristics of these sea echoes can be used to study the HF propagation modes being supported by the ionosphere. This information can then be used to examine the accuracy of ionospheric models used to predict HF propagation characteristics for HF users. This paper describes observations made by TIGER during Spring 2000, and compares them with ray-tracing simulations based on the International Reference Ionosphere.

**Index Terms**—HF propagation, ionosphere, SuperDARN radars

## I. INTRODUCTION

THE aim of the Tasman International Geospace Environment Radar (TIGER) project is to develop two HF ionospheric radars operating at oblique incidence, with intersecting footprints covering the auroral and sub-auroral ionospheres south of Australia and New Zealand (Fig. 1) [1] [2].

The first of the TIGER radars, installed at Bruny Island, Tasmania (147.2°E, 43.4°S geographic;  $-54.6^\circ$  invariant), has been operational since November 1999. Funding is still being sought for the second radar to be located in New Zealand. TIGER is operated by La Trobe University on behalf of a consortium of universities (La Trobe, Monash, Newcastle), government instrumentalities (Australian Antarctic Division, DSTO, IPS Radio & Space Services), and industry (RLM Systems Pty Ltd).

TIGER is also part of the SuperDARN (Super Dual Auroral Radar Network) international network of radars established to provide extensive coverage of both the southern and northern high-latitude ionospheres in order to study the dynamics of high-latitude convection [3] which change dramatically in response to changing conditions in

Manuscript received November 12, 2001. This work was supported by the Australian Research Council, the Australian Antarctic Science Advisory Committee, the Victorian Partnership for Advanced Computing, and the TIGER Consortium Partners.

P. L. Dyson, R. J. Norman, and M. L. Parkinson are with the Department of Physics, La Trobe University, Victoria, 3086, Australia (telephone: 61-3-94792735, e-mail: p.dyson@latrobe.edu.au).

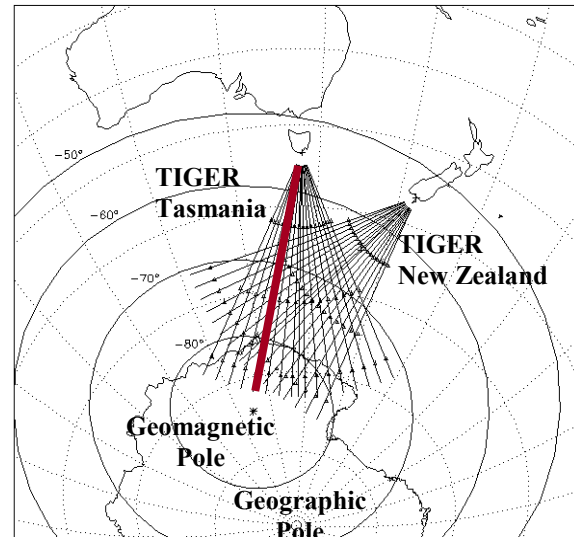


Fig. 1. Field of view of the TIGER Radar. The straight lines represent the 16 azimuthal directions scanned by the  $\sim 3^\circ$  azimuthal beam of each radar. Observations presented in this paper were obtained using beam 4 of the Tasmanian radar, marked in red. The solid curved lines are contours of geomagnetic latitude. The dotted lines are contours of geographic latitude and longitude.

the solar wind as it impacts the Earth's magnetosphere. A consequence of the dynamic nature of the high-latitude ionosphere is the formation of small-scale ionospheric irregularities capable of scattering HF radio waves. TIGER's primary objective is to detect echoes backscattered by these irregularities whenever they occur within the radar beam. However, since HF frequencies can also be reflected back to Earth by the ionosphere, TIGER also detects echoes backscattered from the Earth's surface. Of course, most of these are sea echoes since there is very little land within the TIGER footprint. The situation is illustrated by Fig. 2, which depicts 0.5 and 1.5 hop ionospheric backscatter and 1.0-hop sea scatter. Additional hops can also occur for both types of scatter. The ionospheric irregularities, caused by plasma instabilities, are aligned along the direction of the Earth's magnetic field so ionospheric backscatter occurs when the HF rays are perpendicular to the local magnetic dip angle.

While ionospheric scatter provides the means of studying a wide variety of magnetospheric and ionospheric processes, sea scatter has also proved to be an excellent tool for certain ionospheric studies. For example, atmospheric

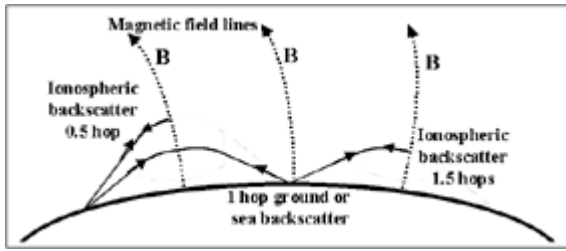


Fig. 2. Schematic of HF rays showing ionospheric and sea backscatter.

gravity waves distort the ionosphere as they travel through it. These larger scale irregularities do not produce direct backscatter but cause focusing and de-focusing of sea echoes as they pass through the ionosphere (e.g., [4], [5]).

Furthermore, since the distribution of sea echoes in range depends on the background ionospheric conditions, it can be utilised to study the general properties of the ionosphere used in making ionospheric predictions for users of the HF spectrum.

This paper describes TIGER sea-echo observations obtained during spring of 2000, defined here as the  $\pm 45$ -day period centred on the spring equinox. The results are compared with the propagation characteristics predicted by the International Reference Ionosphere (IRI) [6].

## II. HF PROPAGATION VIA THE IONOSPHERE

The properties of HF propagation are determined by the spatial structure of the ionosphere. Several modes can exist due to the birefringence caused by the Earth's magnetic

field and the complicated vertical structure. Fig. 3(a) shows schematically some of the typical ionospheric layer structures that can exist depending on the time of day and season. Fig. 3(b) shows typical ray paths on a single HF frequency [7]. At this frequency, propagation via the ionosphere is not possible over ranges less than the skip zone. Note that typically two rays at different elevation angles have the same ground range, but usually the high-angle ray is weaker, and since the length of each ray path is different, the apparent (radar or group) ranges will differ. However, rays with different ground ranges can also have the same apparent range. The situation is even more complicated when more than one ionospheric layer is present, since then several rays may have either the same ground range or the same apparent range.

The expected properties of sea echoes can be modelled by ray tracing through model ionospheres [8], [9]. An example is given in Fig. 4 which shows the simulation of a swept-frequency backscatter ionogram for propagation through a daytime ionosphere consisting of typical E-, F1-, and F2-layers. The clutter (power) levels show the effect of ray divergence due to ionospheric vertical structure. This simulation shows how the group (apparent) range varies with frequency and it illustrates how the larger frequencies propagate to greater ranges, but also have a greater minimum range, or skip distance. Furthermore, echo signatures of the different layers are not distinct but overlap.

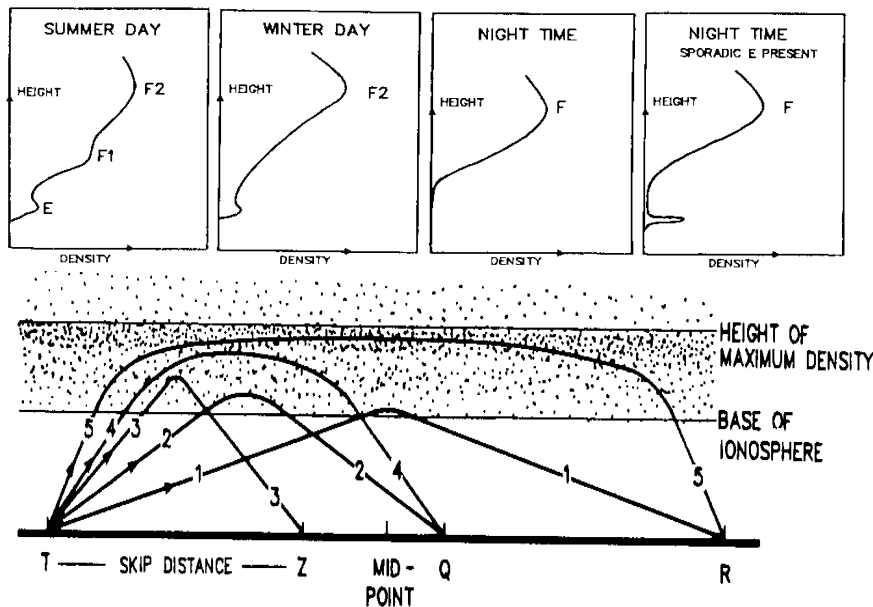
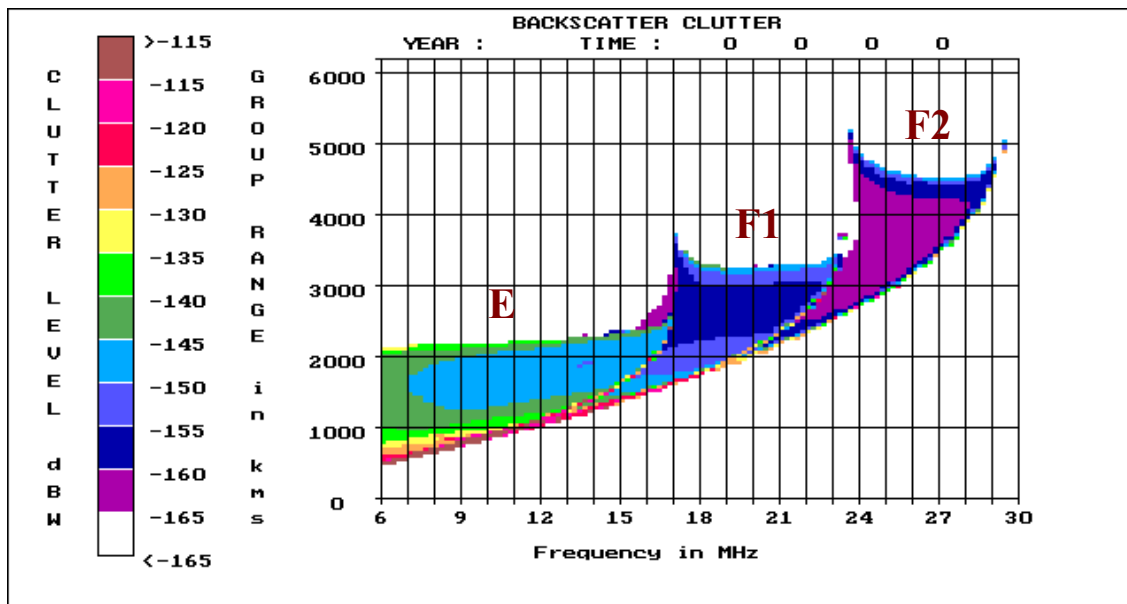


Fig. 3. (a) Top panel shows typical vertical ionospheric profiles, i.e., the variation of electron density with height.(b) Bottom panel shows schematic ray paths for an ionospheric layer (after [7]).



**Fig. 4.** Synthesized backscatter ionogram showing propagation characteristics of ground or sea echoes for an ionosphere containing E, F1, and F2 layers. Ionospheric absorption and antenna patterns have been ignored.

Ignoring the effect of the Earth’s magnetic field the refractive index of the ionosphere,  $\mu$ , is given by

$$\mu^2 = 1 - kN_e/f^2 = 1 - (f_n/f)^2$$

where  $k$  is a constant

$N_e$  is the local electron density

$f_n$  is the local plasma frequency

and  $f$  is the radar operating frequency.

It is apparent that as  $f$  increases,  $\mu \rightarrow 1$ , the free space value, and the amount of ionospheric refraction decreases. As a result, ionospheric refraction is only sufficient to cause reflection if  $f \sim < 3 f_oF2$ , for oblique propagation, where  $f_oF2$  is the maximum plasma frequency of the F2 layer. The results shown in Fig. 4 were obtained using an ionospheric model in which  $f_oF2$  was 9.8 MHz.

Note that because the refractive index depends on the ratio  $f_n/f$ , the frequency scale in Fig. 4 can be regarded as being normalised to  $f_oF2$  through the ratio  $f/f_oF2$ . Thus if the ionospheric model is scaled down by a factor of two so that  $f_oF2$  is halved, the corresponding backscatter ionogram will be the same as in Fig. 4, but with a re-scaled frequency axis covering 3–15 MHz.

Complete simulation of an actual radar system, such as TIGER, requires inclusion of antenna patterns, ionospheric absorption, magnetic field and system losses. A more complete simulation of the TIGER radar has been reported elsewhere [1], [2]. The effects of these additional factors are apparent in a series of swept frequency backscatter ionograms obtained during initial testing of TIGER and an example is shown in Fig. 5. The antenna pattern has a major effect causing the layer signatures shown in Fig. 4 to become bands of echoes whose locations move almost linearly to greater ranges as the frequency increases.

### III. OBSERVATIONS AND INTERPRETATION

In its standard mode of operation, TIGER operates as a fixed frequency sounder, choosing a frequency in the range 8–20 MHz that gives the greatest extent of ionospheric scatter. The choice of frequencies is limited by licence restrictions to a few selected frequency bands so that in practice observations can be grouped into three frequency bands, viz,  $\leq 11$  MHz; 11 to 12.5 MHz; and  $\geq 14$  MHz. As explained above, sea echoes are also observed extensively, and a statistical picture of ionospheric propagation can be built up by counting the sea echoes observed over a period of time. Sea-echo observations obtained during 2000, the first full year of TIGER operation, have been used to examine the diurnal variation in HF propagation for each

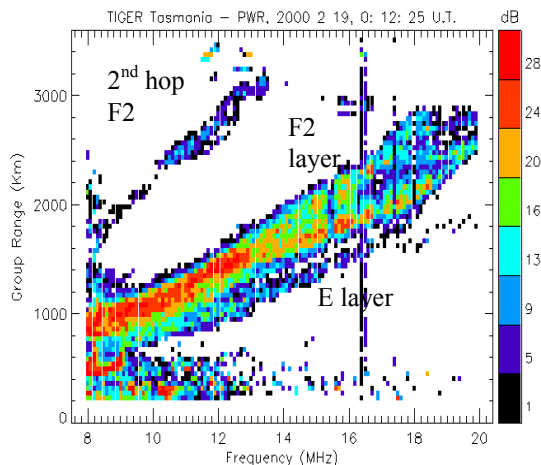


**Fig. 5.** TIGER backscatter ionogram obtained on beam 4 commencing at 00:12:25 UT on 19 February, 2000.

season and this paper presents the results for spring, a season we have studied in more detail.

Fig. 6 shows the percentage of operational time that sea echoes were observed along beam 4 in Spring 2000 when TIGER was operating in the frequency range 11 to 12.5 MHz. Results for the other frequency channels are similar. At high latitudes ionospheric irregularities usually move with velocities greater than those of sea waves. Hence sea echoes are automatically identified as echoes with Doppler shifts indicating line-of-sight speeds  $<50$  m/s. It is possible for slow and fast moving ionospheric irregularities to present small line-of-sight speeds to the radar, and so be misidentified as sea echoes. Generally, the occurrence of such echoes is a secondary consideration, as it is in this study, but their possible impact on results must always be considered.

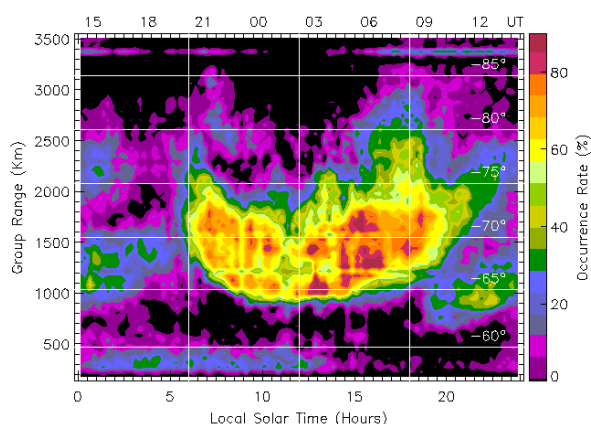


**Fig. 6.** Percentage occurrence of sea echoes observed during Spring of 2000.

The major feature in Fig. 6 is the band of high echo occurrence ( $>60\%$ ) that occurs during local daytime between approximately 900 to 2200 km group range. This feature begins near sunrise at around 1800 km. The leading edge then moves to close ranges reaching a minimum of about 900 km and then moving slowly to greater ranges, finally disappearing just before 2000 LT. The percentage occurrence of sea echoes drops sharply at ranges closer than the leading edge of the 60% contour. The trailing edge of this 60% contour has a similar behaviour in that it moves closer to the radar during the morning hours and retreats after local noon. However, the occurrence drops more slowly beyond this trailing edge and the 40% occurrence contour has excursions to much greater ranges at  $\sim 1300$  LT and  $\sim 1730$  LT. A second feature of relatively high occurrence ( $<40\%$ ) occurs at 700–1200 km between 1900 LT and 0200 LT. Generally, the occurrence of sea echoes between midnight and 0600 LT is  $<30\%$  except occasionally at ranges between 1000–1500 km.

The major daytime feature can be understood in terms of the diurnal variation of  $f_oF2$ . Fig. 7 shows the variation of  $f_oF2$  with local time and range predicted by the IRI for the September equinox, 2000. The range shown is the true (ground) range which, is less than the radar or group range,

but this does not affect the interpretation significantly. The main feature of Fig. 7 is the diurnal variation which is similar at all ranges in that it predicts  $f_oF2$  to be smallest in the early morning hours, then to rise abruptly at about 0600 LT, reach a maximum around 1400 LT, and then decrease significantly after 2100 LT.

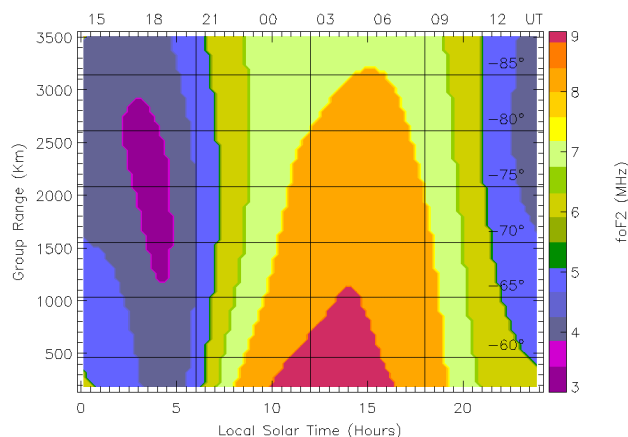


**Fig. 7.** The diurnal variation of  $f_oF2$  given by the IRI model for the beam 4 magnetic meridian at September equinox, 2000.

When operating on a fixed frequency, the ratio  $f/f_oF2$  changes as  $f_oF2$  changes. Thus as  $f_oF2$  decreases, it is equivalent to moving up the frequency scale in Fig. 4, and we can expect the echo signature to move to greater ranges. This is exactly the behaviour shown in Fig. 6 where the band of high occurrence is at greater ranges near sunrise and sunset when  $f_oF2$  is less. Of course, the F2 layer also moves to greater heights during the night. If  $f_oF2$  drops sufficiently low, so that  $f/f_oF2 \sim 3$ , the radar signals will not be reflected by the ionosphere and no sea scatter will be observed. The effects of this are apparent in Fig. 6 which generally shows fewer sea echoes observed at night when Fig. 7 shows that  $f_oF2$  is typically  $\sim 4$  MHz or less. Note that the IRI is a model for magnetically quiet times and during disturbed times  $f_oF2$  may increase. Hence it is not surprising that Fig. 6, which includes magnetically disturbed times, shows non-zero values of occurrence, even when the IRI predicts low values of  $f_oF2$ .

A more detailed comparison was made by ray tracing through model ionospheres obtained from the IRI. The ionosphere was treated as having an isotropic refractive index. Since the ionospheric model contains horizontal as well as vertical gradients, numerical ray tracing was required. The ray divergence was calculated to take account of the effect of ionospheric structure on relative echo power. The method is similar to that described elsewhere [10].

Results for propagation via the F2 layer are presented in Fig. 8, which shows the relative power backscattered from the sea. The variations in power are entirely due to ionospheric effects since we have assumed the changes in sea-wave height due to meteorological factors play a secondary role. We also assume it is valid to compare the

Fig. 8 results with the occurrence plot of Fig. 6 because the latter maps the probability of different ionospheric propagation paths. A direct comparison of the calculated power with the observed average powers requires greater caution because occasionally unrepresentative propagation paths occur which support anomalously small or large backscatter powers. Hence we expect better correspondence between the general features of the power plots for the model ionospheres and the actual occurrence statistics.

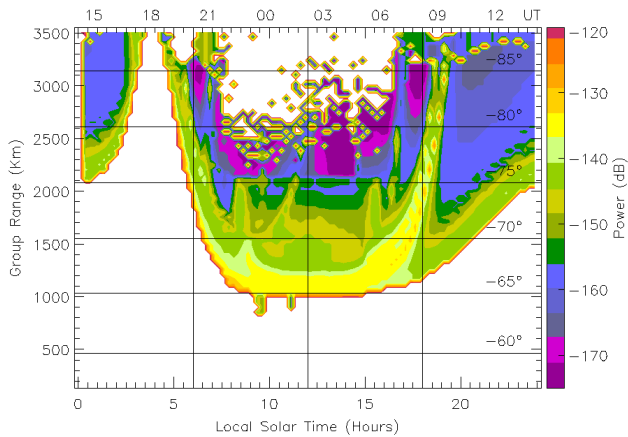


Fig. 8. IRI ray tracing predictions of the power of sea-echoes propagated via the F2-layer for Spring equinox, 2000. Horizontal gradients in plasma density parallel to beam 4 have been included, but not transverse to it.

Indeed there is a good correspondence between the location and behaviour of the leading edge of the daytime echo contours. The main difference is that the ray tracing shows the leading edge continuing into the night and moving to very long ranges in the early morning hours. This behaviour is not evident in the 60% contour in Fig. 6, but it is evident in the 20% contour which extends from 1800 km at midnight to greater ranges at later times and with a gap centred on  $\sim 0330$  (as occurs in Fig. 8). The ray-tracing results show that the rays reaching  $\sim 3000$  km in the early morning hours have low elevation angles  $< 5^\circ$  and the low antenna gain at these angles [11] explains the low or zero occurrence at these ranges in Fig. 6.

The ray-tracing results show that the F2 layer structure causes complicated variations in echo power, which produce ‘tongues’ in the contours extending to greater range. The most pronounced features are just before noon and near sunset ( $\sim 1800$  LT). These features will be modified by the antenna gain but features reminiscent of them appear in the observations, Fig. 6.

Fig. 9 shows  $f_oE$  contours derived from the IRI and Fig. 10 shows the relative power of rays from the ray tracing study that were reflected in the E-region. Both plots are essentially symmetrical about noon and the results show that any E-region echoes will sit within the F2-layer echo trace. The ray tracing gave elevation angles of the E-region rays as  $< 10^\circ$  so the antenna pattern [11] will enhance F2-layer echoes relative to those propagated via the E region. The

IRI also predicts the presence of an F1- layer between 0700 and 1700 LT and layer centred on noon. The power plot of sea echoes propagated via the F1 layer predicted by the ray tracing is similar to that of echoes propagated via the daytime F2 region. Again the F1 echo trace sits within the F2 echo trace so while F1 layer propagation may produce the strongest echoes at some ranges, the overall power contours will not be very different to those predicted by F2-layer propagation alone. Consequently, the main feature in Fig. 6 reflects the properties of F2-layer propagation.

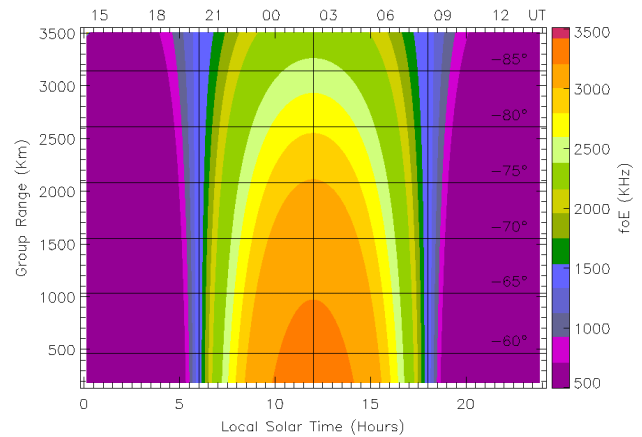


Fig. 9. The diurnal variation of  $f_oE$  given by the IRI model along beam 4 for September equinox, 2000.

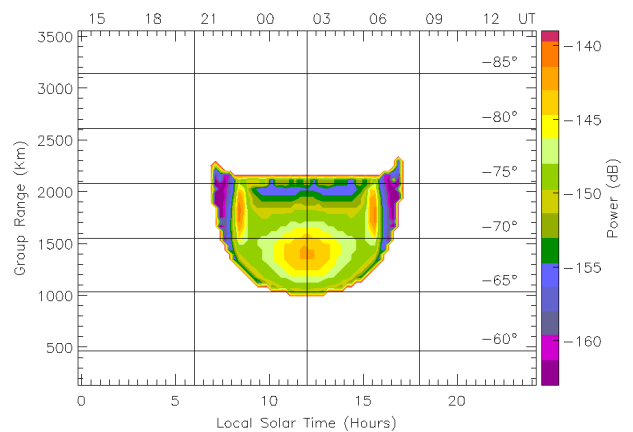


Fig. 10 Sea-echo power simulated by ray tracing through the IRI model for Spring equinox, 2000. These results are for normal E region propagation.

Fig. 6 contains two other main features. The first is the scatter closer than 600 km that extends from  $\sim 2300$  to  $\sim 1300$  LT. The occurrence is centred on dawn and has typical occurrences of  $\sim 20\%$ . We assume this scatter is associated with meteor echoes and it will not be discussed further here.

The second feature begins at  $\sim 1800$  LT at ranges less than 1000 km and continues until 0600 LT, gradually moving to greater ranges. The occurrence rates are typically  $\sim 20\%$  but reach peaks of  $\sim 40\%$ . From reference to Figs 8, 9 and 10, it is apparent that this scatter is not due to normal E- or F2-layer propagation, neither is it due to normal F1-layer propagation. It is therefore explained as being due to

sporadic-E, auroral-Es, or F-layer enhancements associated with geomagnetic activity, all of which are common high-latitude phenomena. From the point of view of communications, it is important to note the relatively high occurrences of these phenomena which models such as the IRI do not attempt to predict.

#### IV. CONCLUSION

Whilst the TIGER radar has been designed to study ionospheric dynamics by detecting backscatter echoes from ionospheric irregularities, the majority of echoes it detects are sea echoes propagated via the ionosphere. These provide a means of examining the HF propagation characteristics of the ionosphere. A comparison of the occurrence statistics of sea echoes observed during Spring of 2000 with ray tracing through model ionospheres obtained from the IRI has shown that the main ionospheric propagation at 11 to 12.5 MHz during this period was F2-layer propagation. The major range-time characteristics of the observations are predicted quite well by the IRI.

The predicted range-time characteristics of normal E-layer and F1-layer propagation overlapped those of the F2-layer propagation so that echoes associated with all three modes are possible. Consequently the preferred mode depends on antenna characteristics, which for TIGER generally gives preference to the F2 mode.

Auroral-E, sporadic-E, and F-layer enhancements associated with geomagnetic activity become very important at night when the sea-echo occurrence is often 20% or higher. These modes support propagation over shorter distances than the F2 mode predicted by the IRI. Therefore, they are an important aspect of HF propagation at high latitudes that are not so readily predicted and many models, such as the IRI, do not even attempt to predict their occurrence.

The study confirms that TIGER and other SuperDARN radars have the potential to provide real-time data useful for HF communicators and prediction services. For example, Hughes et al. [12] have developed a general purpose SuperDARN operation mode designed to provide real-time information of value to the wider community of HF users.

#### ACKNOWLEDGMENTS

We thank the numerous people who contributed to the construction, operation, and maintenance of TIGER. They include John Devlin, Anthony M. Breed, Mark Gentile, Danny Ratcliffe, Paul R. Smith, and Jim Whittington.

#### REFERENCES

- [1] P. L. Dyson and J. C. Devlin, "The TIGER Radar - An Extension of SuperDARN to Sub-auroral Latitudes," *WARS'00 (Workshop on Applications of Radio Science) Proceedings*, (Eds. Dyson and Norman), La Trobe University, pp. 9-31, 2000.
- [2] P. L. Dyson and J. C. Devlin, "The Tasman International Geospace Environment Radar," *The Physicist (The Australian Institute of Physics)*, vol. 37, pp. 48-53, March/April, 2000.
- [3] R. A. Greenwald, et. al., "DARN/SuperDARN: A global view of the dynamics of high-latitude convection," *Space Sci. Rev.*, vol. 71, pp. 761-796, 1995.
- [4] J. C. Samson., R. A. Greenwald, J. M. Ruohoniemi, A. Frey, and K. B. Baker, "Goose Bay radar observations of Earth-reflected atmospheric gravity waves in the high-latitude ionosphere," *J. Geophys. Res.*, vol. 95, pp. 7693-7709, 1990.
- [5] L.-S. He, P. L. Dyson, M. L. Parkinson, and P. J. Wilkinson, "Medium-scale TIDs observed with the TIGER SuperDARN radar," *WARS02 (Workshop on Applications of Radio Science) Proceedings (this issue)*, 2002.
- [6] D. Bilitza, "International Reference Ionosphere 2000," *Radio Sci.*, vol. 36, pp. 261-275, 2001.
- [7] L. F. McNamara, "*The Ionosphere: communications, surveillance, and direction finding*," Kreiger Publishing Company, Florida, USA, 1991.
- [8] P. L. Dyson and J. A. Bennett, "A model of the vertical distribution of the electron concentration in the ionosphere and its application to oblique propagation studies," *J. Atmos. Terr. Phys.*, vol. 50, pp. 251-262, 1988.
- [9] P. L. Dyson and J. A. Bennett, "Exact Ray Path Calculations Using Realistic Ionospheres," *IEE Proceedings-H*, vol. 139, pp. 407-413, 1992.
- [10] C. J. Russell, P. L. Dyson, Z. Houminer, J. A. Bennett, and L. Li., "The effect of large scale ionospheric gradients on backscatter ionograms," *Radio Sci.*, vol. 32, pp. 1881-1897, 1997.
- [11] P. J. Chapman, "Results of modelling the Sabre Communications 608 log periodic antenna using Numerical Electromagnetics code (NEC)," *Proceedings of the SuperDARN Annual Meeting* (Ed. J-C. Cerisier), Reykjavik, Iceland, pp 6.1-6.5, 24-28 May, 1999.
- [12] J. M. Hughes, W. A. Bristow, R. A. Greenwald, and R. Barnes, "Determining HF communications channel parameters using SuperDARN," submitted to *Ann. Geophysicae*, 2001.